Journal of the Korean Nuclear Society
Volume 31, Number 2, pp.236~255, April 1999

An Improved Mechanistic Model to Predict Critical Heat Flux in Subcooled and Low Quality Convective Boiling

Young Min Kwon
Korea Atomic Energy Research Institute
150 Dukjin-dong, Yusong-gu, Taejon 305-353, Korea
ymkwon@nanum.kaeri.re.kr
Soon Heung Chang
Korea Advanced Institute of Science and Technology
373-1 Kusong-dong, Yusong-gu, Taejon 305-701, Korea

(Received November 19, 1998)

Abstract

An improved mechanistic model was developed to predict a convective boiling critical heat flux (CHF) in the vertical round tubes with uniform heat fluxes. The CHF formula for subcooled and low quality boiling was derived from the local conservation equations of mass, energy and momentum, together with appropriate constitutive relations. The model is characterized by the momentum balance equation to determine the limiting transverse interchange of mass flux crossing the interface of wall bubbly layer and core by taking account of the convective shear effect due to the frictional drag on the wall-attached bubbles. Comparison between the present model predictions and experimental CHF data from several sources shows good agreement over a wide range of flow conditions. The present model shows comparable prediction accuracy with the CHF look-up table of Groeneveld et al. Also the model correctly accounts for the effects of flow variables as well as geometry parameters.

Key Words : critical heat flux (CHF), convective boiling, two-phase flow model, wall-bubbly layer

1. Introduction

The physical phenomenon of critical heat flux (CHF) has received considerable attention over the past several decades, because the CHF presents the upper limit coolability of high heat flux components in the design of boiling heat transfer system. For analysis and design purposes, reliable prediction methods are required. However, unfortunately the knowledge is not sufficient to predict the CHF with the desired degree of accuracy. The complication of a CHF problem for forced convection boiling is caused by the large number of variable factors and the variety of two-phase flows. In order to understand the physical nature of the CHF phenomenon, various mechanistic CHF models have been proposed so far.

According to recent reviews about the mechanistic modeling of CHF [1-4], among many existing models available today, only near wall bubble crowding [5-7] and liquid sublayer dryout [8-10] models are receiving attention for the prediction of the CHF in the moderate and highly subcooled conditions. However, comparative analyses [11-13] show that the predictive capabilities of all the existing mechanistic CHF models are not enough to apply them to new system designs.

The near wall bubble crowding model was first developed by Weisman and Pei [5]. The model is based on the existence of a bubbly layer adjacent to the heated surface. It assumes that CHF occurs when the void fraction of the bubbly layer reaches a critical value, because bubble crowding prevents the bulk cold liquid from reaching the wall. Turbulent interchange between the bubbly layer and core is the limiting mechanism of the onset of CHF. While the liquid sublayer dryout model, first proposed by Lee and Mudawar [8], is based on the existence of vapor slug adjacent to the tube wall. It assumes that CHF occurs at the dryout condition of the thin liquid layer beneath a vapor slug that is generated by Helmholtz instability at the interface between the liquid layer and vapor region. Both types of CHF models are capable of providing reasonably accurate predictions being very close when compared with each other.

Chang and Lee [14] proposed a mechanistic CHF model based on the same concept of Weisman and Pei, while the CHF formula was derived from mass, energy and momentum balance equations. The limiting transverse mass flux crossing the interface of the bubbly layer and core was determined from a momentum balance. Compared to other mechanistic models, the predictions against experimental data are known to be somewhat less accurate. Lee et al. [15] revised the original model with fixing mistakes included in the momentum balance, which were pointed out by Bricard and Souyri [13], and they revised the model by introducing several new constitutive relations.

In this paper, a two-phase flow model for the subcooled and low quality boiling is presented, where some significant modifications are made on the physical concept of the CHF mechanism and the relevant constitutive relations in the bubble crowding model. Because the reasoning of Chang and Lee's model, in the author's opinion, provides a sound starting point, the present model utilizes its analytical frame. The proposed model is validated on the experimental CHF data of water in uniformly heated tubes over a wide range of parameters and compared with the prediction using the Ying and Weisman [6] model and the CHF look-up table of Groeneveld et al. [16].

2. Two-Phase Model of CHF

2.1. Physical System and Basic Assumptions

Most of the existing mechanistic models are based on the hypothetical flow structure or the limited experimental observation at CHF condition. Attempted in this study is the development of a new prediction model of the convective boiling CHF based on the suggested wall-attached bubbles layer or wall bubbly layer. A physical image of the boiling structure considered in this study is shown in Fig. 1, where the transverse interchange crossing the interface of the wall bubbly layer and core is shown. The flow is divided into two regions. In the outer annular layer of the round tube, attached bubbles are packed on the wall just prior to agglomeration and in the middle of the tube is a mixture core consisting of liquid and bubbles. The flow structure is based on the experimental observation by

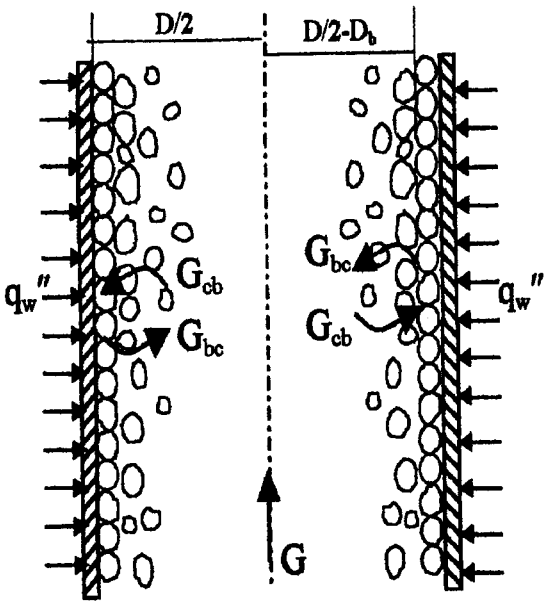

Fig. 1. Conceptual Configuration of Bubbles on the Heated Wall

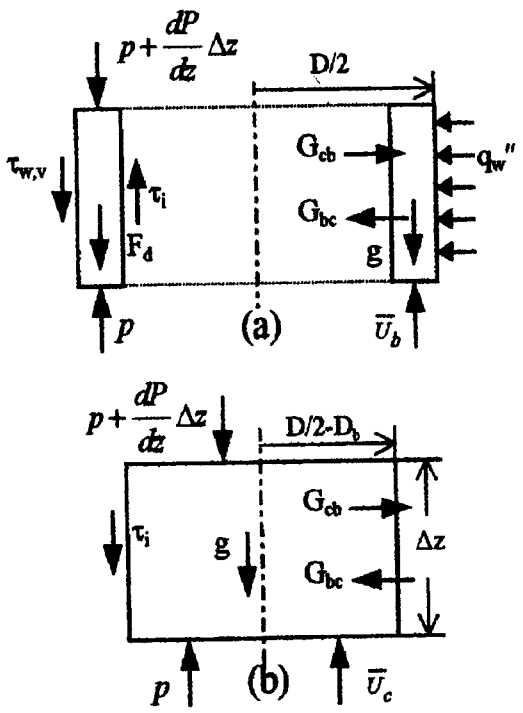

Fig. 2. Separated Flow Control Volumes for (a) Wall Bubbly Layer and (b) Core Region

Gunther [17] and Kirby et al. [18] that the two-phase layer of local vapor film in the subcooled flow boiling was an order of one bubble thickness. The present study uses the general approach of Weisman and Pei [5]. However, the effective thickness of bubbly layer is considered as a single bubble diameter, because it is assumed that only the wall-attached bubbles play the effective physical barrier to the heat transfer from the wall and the liquid supply from the core. Yagov et al. [19] adopted a similar configuration of bubbly layer with a single bubble thickness for their semi-empirical CHF model under highly subcooled condition.

According to Saha and Zuber [20], at low mass flow rates, bubble detachment from the wall is thermally controlled and independent of hydrodynamic forces. While at high mass flow rates, bubbles do not easily detach from their nucleation sites because bubbles are small enough to prevent bubble detachment from the wall by the hydrodynamic forces. Therefore, the wall-attached bubbles form a wall bubbly layer, which acts as a wall roughness. Bubble departure depends on the drag force, which, in turn, depends upon the characteristic skin friction experienced by the wall bubbly layer. Once the drag and buoyancy forces are strong enough to overcome the surface tension force that holds the bubbles to the wall, the bubbles tear free, and move immediately into the core.

Generally, active nucleation site density drastically increases when heat flux approaches to the CHF. It is assumed that bubbles are packed in a most dense array on the wall at near CHF condition. Then the CHF is assumed to reach at a certain void fraction in the bubbly layer (called critical wall-void fraction) when radial thermal transport is limited by equal flows inward and

outward at the interface of the wall bubbly layer and core. If the wall heat flux exceeds the maximum permissible heat flux satisfying the limiting condition above, the liquid in the wall bubbly layer depletes then dry spot area rapidly increases, and consequently the CHF occurs. The thermal transport limitation is governed by local mass, energy, and momentum balance equations based on the assumption that the subcooled flow boiling CHF is a local phenomenon. The limiting transverse interchange of mass flux crossing the interface of the wall bubbly layer and core is determined by a momentum balance equation.

Beattie [21] has shown that the wall-attached bubbles act as a surface roughness equivalent to bubble size. Under such a condition, the friction factor can be described by the same form of equation as that used for a single-phase flow in roughened tubes. Although Beattie considered the flow remote from the CHF, it can be supposed that bubbles in the CHF region behave similarly. Also, for predicting the pressure drop in the subcooled flow boiling channel, Jia and Schrock [22], and Lu and Jia [23] proposed mechanistic models based on the enhanced friction coefficient due to the wall-attached bubbles. It was reported that their models could give a satisfactory agreement with experimental data. In the present work, the wall-attached bubbles are considered as increasing the roughness of the tube. The existence of roughness changes the hydrodynamic characteristics of the flow and the effect of viscous shear due to molecular friction becomes relatively small.

2.2. Conservation Equations

In the present study, one-dimensional subcooled flow boiling in a tube is analyzed with two-phase flow models and constitutive equations. The basic assumptions of the present model for mathematical formulation are: (1) Two-phase flow structure at near CHF condition always takes the form of semi-reversal-annular flow pattern as shown in Fig. 1. (2) The flows in the core and wall bubbly layer are each homogeneous. (3) The flow is steady. (4) The axial change of pressure is negligible compared with the system pressure. (5) Thickness of the wall bubbly layer is very small compared to the tube radius.

The governing equations are derived by applying the basic local conservation rules for mass, energy, and momentum to the control volumes such as that shown in Fig. 2. Considering the wall bubbly layer control volume of Fig. 2(a), total mass and energy balances are given as below, respectively.

$$\frac{dG_b A_b}{dz} + G_{bc}\xi_i - G_{cb}\xi_i = 0 \tag{1}$$

$$\frac{dG_b A_b h_b}{dz} + G_{bc} h_b \xi_i - G_{cb} h_c \xi_i - q''_w \xi_w = 0 \tag{2}$$

G_{cb} and G_{bc} are the total inward and outward mass fluxes at the interface of the wall bubbly layer and core. ξ_i and ξ_w are the perimeters of the interface and the heated wall, respectively, i.e., $\xi_i = \pi(D-2D_b)$ and $\xi_w = \pi D$, where D_b is the detached bubble diameter determined by the subcooled flow boiling model. Considering the relation of h_b in Eq. (14), two equations of (1) and (2) can be combined into Eq. (3). The variation of saturation properties of liquid and vapor in the axial flow direction is neglected because the pressure drop along the tube is small compared to the system pressure. Since the critical wall-void fraction α_b is limited at the CHF condition, the quality in that layer has a finite value, i.e., $dx_b/dz = 0$, with the assumption of homogeneous flow.

$$q''_w = G_{ch}(h_b - h_c)\frac{\xi_i}{\xi_w} \tag{3}$$

For comparing with the CHF formula of Weisman and Pei [5], a liquid mass balance on the wall bubbly layer is considered.

$$\frac{dG_b(1-x_b)A_b}{dz}+\frac{q''_{evap}\xi_w}{h_{fg}}+G_{bc}(1-x_b)\xi_l-G_{cb}(1-x_c)\xi_l=0 \quad (4)$$

where q''_{evap} represents the portion of wall heat flux that goes into the net formation of vapor that enters the core. Two mass balance equations of (1) and (4) can be combined as below:

$$q''_{evap}=G_{cb}(x_b-x_c)h_{fg}\frac{\xi_l}{\xi_w} \quad (5)$$

By introducing the factor F_q, representing a fraction of the heat flux producing vapor that enters the core, we obtain Eq.(6) from Eqs.(3) and (5). Eq.(6) is the same equation derived by Weisman and Pei.

$$q''_w=\frac{q''_{evap}}{F_q}=\frac{q''_{evap}(h_b-h_c)}{(x_b-x_c)h_{fg}} \quad (6)$$

The qualities appeared in the above equations are the actual flow qualities based on a nonequilibrium condition and x_b is the quality corresponding to the critical wall-void fraction α_b. It should be noted that the general approach to determine the boiling heat flux by using of mass and energy balances on the bubbly layer is the same as done by Weisman and Ileslamlou [7].

It is assumed that the wall-attached bubbles act as a surface roughness equivalent to bubble size. Chen [24], and Taylor and Hodge [25] reported that the flow resistance of a rough surface is divided into two components - that due to the form drag on the roughness element and that due to the viscous shear on the smooth surface area between the roughness elements. Based on the one-dimensional momentum equation of a separated flow model, momentum balances between shear forces, frictional drags, and pressure on the control volumes of the wall bubbly layer (Fig. 2(a)) and core (Fig. 2(b)) are written, respectively, as:

$$-\frac{dP}{dz}+\frac{\tau_i\xi_i}{A_b}-\frac{\beta\tau_{w,v}\xi_w}{A_b}-\frac{F_dN_{bub}}{A_b dz}-\rho_b g+\frac{(G_{cb}\bar{U}_c-G_{bc}\bar{U}_b)\xi_i}{A_b}=\frac{1}{A_b}\frac{d}{dz}(\rho_b\bar{U}_b^2A_b) \quad (7)$$

$$-\frac{dP}{dz}-\frac{\tau_i\xi_i}{A_c}-\rho_c g+\frac{(G_{bc}\bar{U}_b-G_{cb}\bar{U}_c)\xi_i}{A_c}=\frac{1}{A_c}\frac{d}{dz}(\rho_c\bar{U}_c^2A_c) \quad (8)$$

The number of attached bubbles along dz in the bubbly layer is, $N_{bub}=\pi Ddz/D_b^2$, where bubbles are arranged in a rectangular lattice with a pitch of D_b. As in Taylor and Hodge, the apparent wall shear stress τ_w is defined as the sum of the viscous shear $\tau_{w,v}$ and form drag on the wall. F_d is the drag force which the rough element of a single bubble exerts on the flow field, and $\beta(0<\beta<1)$ is the blockage factor that represents the area of the smooth surface between bubbles that is open for flow. As a first approximation, the drag force exerted on a single bubble is assumed to be $F_d \sim \lambda \rho_c U_c^2/2\times(\pi D_b^2/4)$, which is the same approach as done in Staub' s [26] subcooled boiling model.

Subtracting Eq. (7) from Eq. (8) to eliminate the pressure gradient term in the left-hand side, we obtain the limiting transverse interchange of mass flux at the interface of the wall bubbly layer and core.

$$G^*=\left[\frac{-\tau_i\xi_i}{\eta_c(1-\eta_c)A}+\frac{\beta\tau_{w,v}\xi_w}{(1-\eta_c)A}-(\rho_c-\rho_b)g+\frac{\pi DF_d}{D_b^2(1-\eta_c)A}+\Phi_{acc}\right]\frac{A\eta_c(1-\eta_c)}{(\bar{U}_c-\bar{U}_b)\xi_i} \quad (9)$$

with the definitions of the acceleration term.

$$\Phi_{acc}=\frac{1}{A_b}\frac{d}{dz}(\rho_b\bar{U}_b^2A_b)-\frac{1}{A_c}\frac{d}{dz}(\rho_c\bar{U}_c^2A_c) \quad (10)$$

The fraction of cross-section occupied by core is expressed by $\eta_c=A_c/A$. At CHF condition, the transverse mass transport rate at the interface is limited, i.e., $G^* = G_{bc} = G_{cb}$. Because the bubble departure diameter is much smaller than the tube radius, variation of shear stress across the thin wall

bubbly layer can be neglected, i.e., $|\tau_l| \cong |\tau_{w,v}|$. If we assume that the wall bubbly layer behaves like the boundary layer region in a single-phase pipe flow, then the wall shear stress $\tau_{w,v}$ can be calculated from the Newton' s viscous law using the universal velocity profiles. According to the rough calculation, the effects of shear stresses are negligible compared to the other terms in the bracket of Eq. (9) for both cases of β=0 and 1. The detail of velocity profile is described in section 2.3.4.

Also, Chang and Lee [14] have shown that the acceleration term Φ_{acc} is negligibly small with respect to the radial mixing flow effect. Therefore, for simplicity in this calculation, the first and second shear stress terms, and the acceleration term in the bracket of Eq. (9) are disregarded. This approach may seem crude, but the results are not strongly affected by the simplified assumption. Finally the CHF formula is expressed as a simple form from Eqs. (3) and (9).

$$q''_{CHF} = \left[-(\rho_c - \rho_b)g + \frac{\pi D F_d}{D_b^2(1-\eta_c)A}\right] \frac{\eta_c(1-\eta_c)(h_b - h_c)A}{(\bar{U}_c - \bar{U}_b)\xi_w} \quad (11)$$

As shown in Eq. (11), accurate prediction of flow enthalpy at the location of the CHF occurrence is very important. In the case of uniform heating, the CHF usually occurs at the end of the heated tube. Assuming homogeneous flows of the wall bubbly layer and core, the quantities at the tube exit are defined as below:

$$\alpha_c = \frac{1}{\eta_c}\alpha_{avg} - \frac{1-\eta_c}{\eta_c}\alpha_b \quad (12)$$

$$h_c = h_l(1-x_c) + h_g x_c \quad (13)$$

$$h_b = h_f(1-x_b) + h_g x_b \quad (14)$$

$$\rho_c = \rho_l(1-\alpha_c) + \rho_g \alpha_c \quad (15)$$

$$\rho_b = \rho_f(1-\alpha_b) + \rho_g \alpha_b \quad (16)$$

$$\mu_{2\phi} = \mu_f(1-\alpha_{avg})(1+2.5\alpha_{avg}) + \mu_g \alpha_{avg} \quad (17)$$

The average viscosity of core region $\mu_{2\phi}$ is evaluated by Beattie and Whalley [27]. The void fractions of the wall bubbly layer and core are represented by α_b and α_c, respectively. The average bulk void fraction α_{avg} is determined by Eq.(25).

2.3. Constitutive Relations

In order to achieve closure of the mass, energy and momentum balance equations, additional constitutive relations are required. As known well, the accuracy of calculation results by the two-phase flow model is dependent on the utilized constitutive relations. Prediction accuracy of existing theoretical CHF models are dependent on the limited applicability of various constitutive relations employed within them as well as empirical constants. All equations utilized in the present model are presented in Appendix I.

2.3.1. Critical Wall-Void Fraction

The bubbly layer thickness is a characteristic parameter in the bubble crowding model, and it was assumed to be 2.5 times of bubble diameter by Weisman and Pei [5] and 1.7 times by Chang and Lee [14]. The thickness was determined empirically by best fitting the CHF model to a large number of data points. In the present study, the effective thickness of wall bubbly layer is assumed to be single bubble diameter, which eliminates the need of such an empirical constant.

The critical wall-void fraction α_b is defined as a volume fraction of steam in the wall bubbly layer at which CHF occurs. In most practical analyses, the

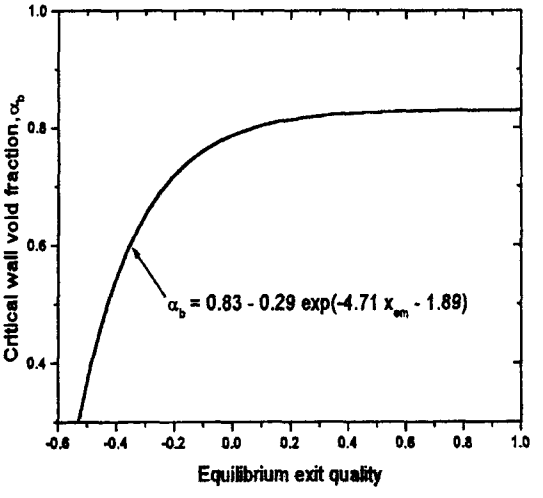

Fig. 3. Correlation of Critical Wall-void Fraction

underlying task in the bubbly crowding model is to determine the α_b. However, an information of α_b is quite limited both experimentally and theoretically until now. At this point, we have no better evidence to utilize anything other than the simple expression by experimental data fitting. By recognizing that the void fraction in the wall region is a function of the bulk flow void fraction, the relationship between α_b and exit equilibrium quality x_{em} is established, as a first approximation, in collaboration with experimental CHF data. Since the bulk void fraction is sensitive to the subcooled flow boiling model utilized in the calculation, the α_b is correlated with the thermal equilibrium quality, which is calculated from the initial condition with heat balance. The final choice of α_b incorporated in the present model is shown by the curve in Fig.3, where it is approximately correlated by the following relation.

$$\alpha_b = 0.83 - 0.29\exp(-4.71x_{em} - 1.89) \quad (18)$$

It is worth noting that values of 0.82 and 0.75 were utilized for the α_b by Weisman and Pei, and Chang and Lee in their CHF models, respectively. As shown in Fig.3, the α_b approaches the similar value (0.83) of the Weisman and Pei's model as exit quality increases. This equation is valid for the average bulk void fraction at the CHF occurrence (tube exit in this work) is not greater than 0.8, otherwise the flow structure of Fig. 1 can not be maintained.

2.3.2. Bubble Detachment Point and Detached Bubble Diameter

Reliable predictions of the point of onset of bubble departure (OBD) and the detached bubble diameter are of essential for the prediction of CHF in Eq. (11). The two terms of OBD and the onset of significant vapor generation (OSV) are usually used to mean the same point. The Levy's model [28] is employed in the present study. According to the critical review by Lee et al. [29], in which the prediction methods were reviewed and compared with extensive data, the model of Levy was found to be the best one to fit with the whole set of data among the analytical models considered. For the relative roughness parameter of tube ϵ/D, a value of 10^{-4} was used by Levy. Once the subcooling required for the OBD, $\Delta h_{sub,d}$, is known, the equilibrium quality at that point, x_d, is thus calculated.

The bubbles grow up on the surface, detach and new bubbles grow again, so that the system is not a steady state in reality. For simplicity, the time-averaged diameter of the growing bubble is assumed as the bubble departure diameter. The bubble diameter at the OBD can be determined from a balance of the fluid forces acting on the bubble and the surface force, and Levy [28] expressed it as:

$$D_h = 0.015\sqrt{\frac{8\sigma D\rho_{avg}}{fG^2}} \quad (19)$$

For some high heat flux situations, the liquid enthalpy at the tube inlet is already above the value of $\Delta h_{sub,d}$. For this case, bubbles are assumed to start growing at the tube inlet.

2.3.3. Friction Factor Model of the Wall-Attached Bubbles

Chang and Lee [14] used the friction factor model of Nedderman and Shearer [30] with the idea that the bubble layer might behave like the regular sand roughness used by Nikuradse in his experiment. However, the bubbly layer probably acts more like the random roughness found in commercial tubes and piping, because the bubbles are growing and collapsing on the heated wall. Therefore, the turbulent skin friction coefficient λ is calculated using the Colebrook-White equation with a two-phase Reynolds number, $Re_{2\phi}=GD/\mu_{2\phi}$, to account for the variation of the fluid viscosity near the heated wall, which is defined as:

$$\frac{1}{\sqrt{\lambda}} = 3.48 - 4\log\left(\frac{2D_h}{D} + \frac{9.35}{\mathrm{Re}_{2\phi}\sqrt{\lambda}}\right) \tag{20}$$

2.3.4. Average Velocities of the Wall Bubbly Layer and Core

The average fluid velocity of the wall bubbly layer $\overline{U}_b$ is determined by taking it as half the velocity of the core at the outer edge of the wall bubbly layer, because the velocity profile in the bubbly layer is near linear. That assumption is valid for the case that the thickness of the wall bubbly layer is much smaller than the tube radius.

$$\overline{U}_b = 0.5U_c(at\ y = D_b) \tag{21}$$

where y is a distance from the wall in the radial direction. The universal logarithmic velocity profile for a single-phase turbulent flow proposed by Karman is assumed to be valid in the turbulent core region.

Once the average velocity of the wall bubbly layer is determined from Eq. (21), the average velocity of core can be calculated as:

$$\overline{U}_c = \frac{G - \overline{U}_b\rho_b(1-\eta_c)}{\rho_c\eta_c} \tag{22}$$

with the constant mass flow rate condition.

$$G = G_c\eta_c + G_b(1-\eta_c) \tag{23}$$

2.3.5. Nonequilibrium Flow Quality and Void Fraction

The flow quality and void fraction in the subcooled flow boiling can be evaluated by both the profile-fit and mechanistic approaches [31]. Two distinctly different approaches are well described in the book by Lahey and Moody [32]. Because little difference in the CHF predictions appeared when both methods were applied to the present CHF model, the simple profile-fit method of Saha and Zuber [20] was employed. The profile-fit method is normally easier to use than the mechanistic method and is as accurate for steady-state calculation. The relationship between the true flow quality x_{avg} and the thermodynamic equilibrium qualities is expressed by:

$$x_{avg} = \frac{x_{em} - x_d\exp(x_{em}/x_d - 1)}{1 - x_d\exp(x_{em}/x_d - 1)}, \tag{24}$$

where x_d and x_{em} are thermodynamic equilibrium qualities determined at the OBD point and tube exit, respectively.

Once the flow quality at the tube exit is determined using Eq. (24), the average bulk void fraction α_{avg} is calculated using the Zuber and Findlay model, modified by Dix [33], that is reasonably accurate for many practical

Table 1. Experimental Conditions of CHF Data Selected for Comparison

Parameter Reference	No.	D (m)	L (m)	P (MPa)	G (kg/m^{2}s)	Δh_{in} (kJ/kg)	X_{em}	q''_{CHF} (kW/m^2)
Thompson & Macbeth (1964)	1122	0.0011 ~ 0.038	0.035 ~ 1.97	2.14 ~ 18.96	496 ~ 7499	2.0 ~ 1659	-0.49 ~ 0.41	760 ~14800
Becker et al. (1971)	804	0.004 ~ 0.02	0.4 ~ 4.97	3.04 ~ 20.0	452 ~ 7438	60 ~ 1372	-0.31 ~ 0.60	135 ~ 7480
Zenkevich (1974)	2925	0.005 ~ 0.011	1.0 ~ 6.0	5.89 ~ 19.62	497 ~ 6694	5 ~ 1621	-0.49 ~ 0.62	137 ~ 7290
Tong (1964)	123	0.006 ~ 0.013	0.38 ~ 3.66	5.17 ~ 13.79	678 ~ 7499	27 ~ 1060	0.00 ~ 0.38	760 ~ 5900
Mayinger (1967)	35	0.007	0.56 ~ 0.98	7.0 ~ 10.24	2255 ~ 3734	0 ~ 278	0.098 ~ 0.21	924 ~ 2860
Total	5009	0.0011 ~ 0.038	0.035 ~ 6.0	2.14 ~ 20.0	452 ~ 7499	0 ~ 1659	-0.49 ~ 0.62	135 ~ 14800

applications. Zuber and Findlay [34] first proposed the void fraction based on the drift flux model as follows:

$$\alpha_{avg} = \frac{x_{avg}}{\left\{C_o\left[x_{avg} + \frac{\rho_g}{\rho_l}\left(1 - x_{avg}\right)\right] + \frac{\rho_g V_{gj}}{G}\right\}} \tag{25}$$

with

$$V_{gj} = 2.9\left[\frac{\left(\rho_l - \rho_g\right)\sigma_l g}{\rho_l^2}\right]^{1/4} \tag{26}$$

In an attempt to relate C_o and V_{gj} to the void fraction, Dix suggested a functional form for the distribution parameter C_o.

3. Verification of the CHF Model

3.1. Procedure of CHF Prediction

The procedure of CHF prediction is as follows. For the given geometry of a tube, the conditions of pressure, inlet flow rate, and inlet subcooling are fixed, then the assumed heat flux to the tube wall is varied until the heat fluxes of the assumed and the calculated by Eq.(11) converge into one value. Since the model presented in this paper is complicated, the CHF calculation procedure is presented in Appendix I.

Predictions using the present theoretical CHF model are compared with the experimental CHF data by examining the statistical results of CHFR, defined as the predicted CHF to the measured CHF. The three statistical parameters of μ (average value), σ (sample standard deviation), and *RMS* (root-mean-square error) of CHFR are utilized.

3.2. Comparisons with Experimental Data

To assess the predictive capability and the limitation of the proposed model, a total of 5009 water CHF data points, covering a wide range of different parameters, was obtained from the KAIST CHF database [35]. The database comprises of about 15000 data for water flow in uniformly heated vertical round tubes compiled from various sources. The range of parameters for

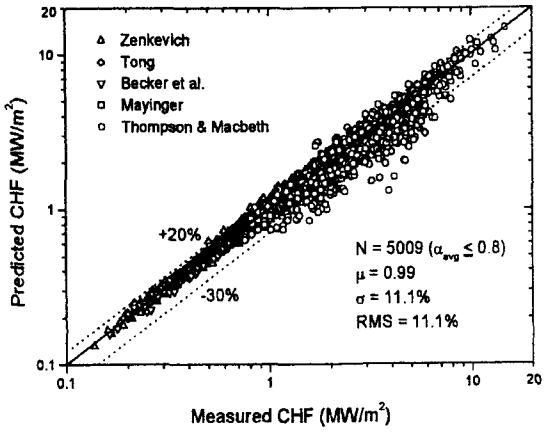

Fig. 4. Predicted vs Experimental CHF

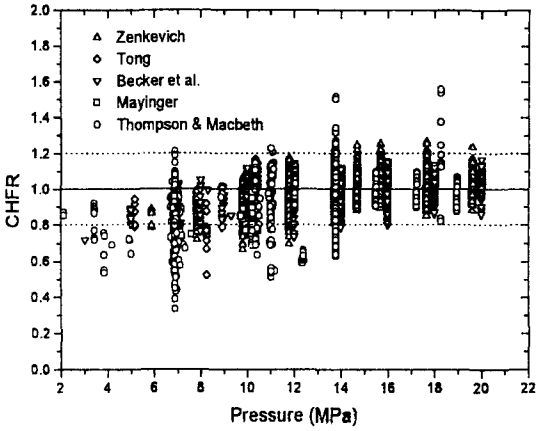

Fig. 5. CHFR vs Pressure

each data source [36-40], considered in this study, is presented in Table 1. These data points satisfies the condition that the average bulk void fraction at the tube exit is not greater than 0.8 to ensure maintaining the flow structure of Fig.1. The selection of data points from the experimental database was conducted by using the subcooled flow boiling model before CHF calculation. The parameter ranges of the selected data points are diameters from 1 to 37.5 mm, lengths from 0.035 to 6 m, mass fluxes from 450 to 7500 kg/m^{2}s, pressures from 2 to 20 MPa, inlet subcooling from 0 to 1660 kJ/kg, and critical heat fluxes from 135 to 14800 kW/m^2, which covers the operating ranges of typical light water reactor (LWR).

A set of the α_b as a function of x_{em}, resulting in an average CHFR of 1.0 while minimizing *RMS* error, were investigated by varying its value against the data points of Table 1. As a result, the correlation of Eq. (18) was obtained. In Fig. 4 the comparisons of the predicted and measured CHF using the above data set are very encouraging. Most of the experiment data (about 93%) are successfully predicted within $\pm$20% error band. The standard deviation σ and *RMS* error of CHFR are 11.12% and 11.14%, respectively. Some data points of Thompson and Macbeth [38], and Tong [39], however, deviate from the error range, which may be considered as typical uncertainties associated with experiments. It should be noted that even though Hall and Mudawar [41] found several problems in the database of Thompson and Macbeth, no examination was conducted to re-evaluate all their data in this study. Most of the deviating data from $\pm$20% error band belongs to their database. If we restrict the application range of exit void fraction less than 0.7, about 97% of the total 3498 data is predicted within $\pm$20%, with μ = 1.02, σ = 8.91%, and RMS = 9.2%, while 99% data is predicted within $\pm$30% error band.

The dependence of the prediction accuracy on major parameters is presented in Figs. 5-8, where the CHFR is plotted versus pressure P, mass flux G, exit void fraction α_{avg}, and ratio of tube length-to-diameter L/D, respectively. A comparison of theoretical predictions by the present CHF model with experimental data does not seem to exhibit significant systematic deviations which could be attributed to a certain system parameter, such as thermal hydraulic conditions and geometric

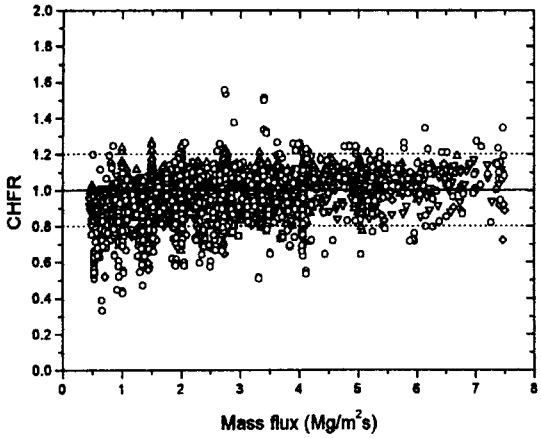

Fig. 6. CHFR vs Mass Flux

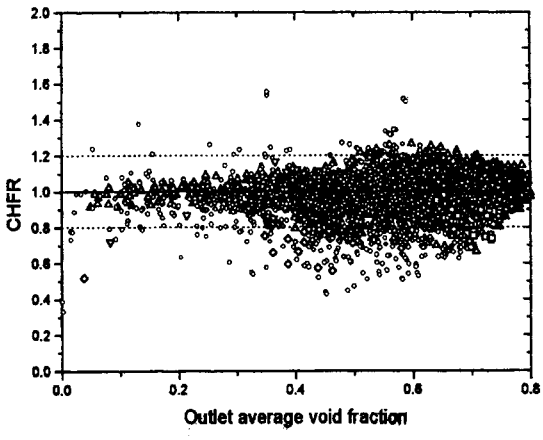

Fig. 7. CHFR vs Average Bulk Void Fraction

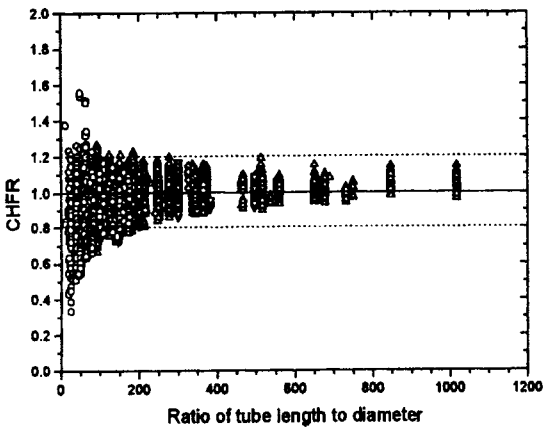

Fig. 8. CHFR vs Ratio of Tube Length to Diameter

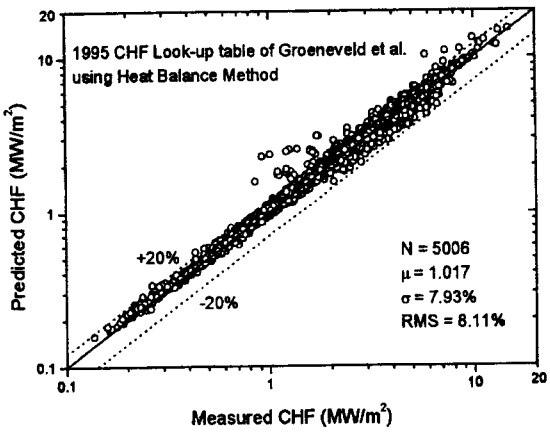

Fig. 9. CHF Prediction by the Look-up Table of Groeneveld et al.

parameters. However, the predictions at the low pressure (less than 7 MPa) and low mass flux (less than 1500 kg/m²s) regions are generally underestimated as shown in Figs. 5 and 6.

For comparing with the present model, the predictions using the CHF look-up table of Groeneveld et al. [16] and the Ying and Weisman [6] model were performed. The so-called heat balance method (HBM) was applied to the look-up table method. Because the look-up table has its applicable ranges, 5006 out of 5009 data points were used for comparison. For tubes of diameter other than referenced 8 mm, the diameter correction rule suggested by the table authors was used. Figs 9 and 10 show the comparisons of experimental data points with two predictions, respectively. The Ying and Weisman model has a tendency to overpredict the CHF as shown in Fig.

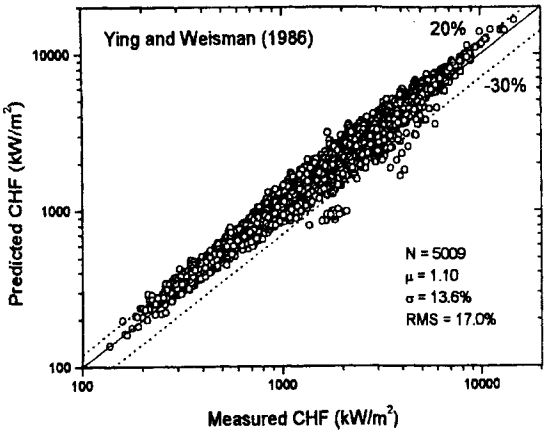

Fig. 10. CHF Prediction by the Ying and Weisman's Model

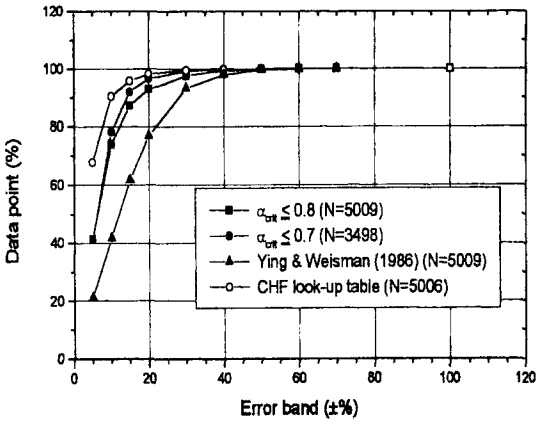

Fig. 11. Percentage of Data Points Predicted Within Error Band

10. The percentage of data points calculated with a given error band (±%) for different prediction methods is presented in Fig. 11. The prediction accuracy of the look-up table is best among the prediction methods considered, and the present model is better than the model of Ying and Weisman. However, for subcooled conditions when the equilibrium quality at the tube exit is less than zero, the prediction accuracy of the present model [42] is better than the CHF look-up table. About 96% of the total 902 data is predicted within ±20% error band, with μ = 0.995, σ = 8.75%, RMS = 8.76%, respectively. While the Lookup table of Groeneveld et al. predicts 93% of the 899 data within ±20%, with μ = 1.02%, σ = 10.97%, RMS = 11.12%, respectively.

3.3. Parametric Trends of the System Variables

Fig. 12 shows that the parametric trends of CHF predicted by the present model are in good agreement with the data of Weatherhead [43]. Also shown in Fig. 12 is the influence of inlet subcooling on CHF in the relatively high pressure region (13.8 MPa). The CHF increases almost linearly with inlet subcooling but its effect decreases with decreasing mass flux. The trends agree with general understanding regarding the CHF characteristics. The effect of liquid subcooling on CHF is prominent because the subcooled liquid flow condenses steam bubbles and suppresses their coalescence on the wall.

Fig. 13 shows the effect of mass flux on CHF with the pressure as another independent variable, where CHF increases with increasing mass flux. The effect of mass flux depends on the system pressure such that it is stronger at lower pressure regions. The experimental data in Fig. 13 are directly taken from the CHF look-up table of Groeneveld et al. [16] for an 8 mm diameter tube based on reference exit quality, x_{em} = -0.2.

The effect of tube diameter on CHF is predicted by the present model, together with the interrelation between tube diameter and inlet subcooling as shown in Fig. 14. The CHF increases with increasing tube diameter at fixed inlet conditions. The effect increases with the increase of the inlet liquid subcooling. Because the CHF look-up table presents CHF values for 8 mm

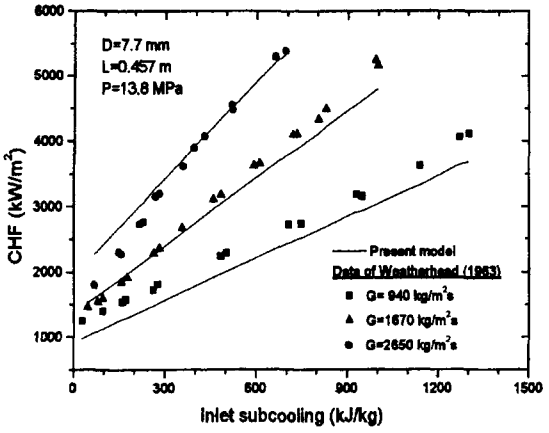

Fig. 12. Comparison of Predicted CHF with Experimental Data of Weatherhead(1963)

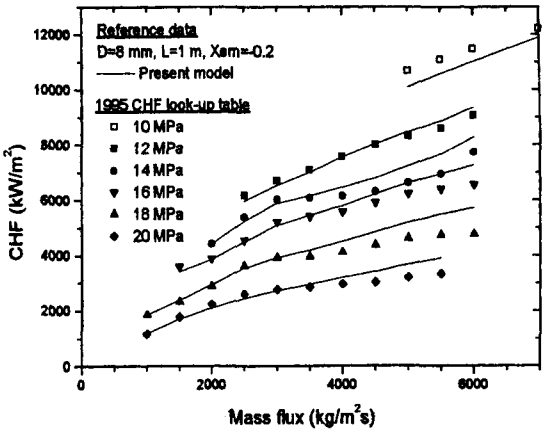

Fig. 13. Prediction of Mass Flux Effect on CHF Compared with the 1995 CHF Look-up Table

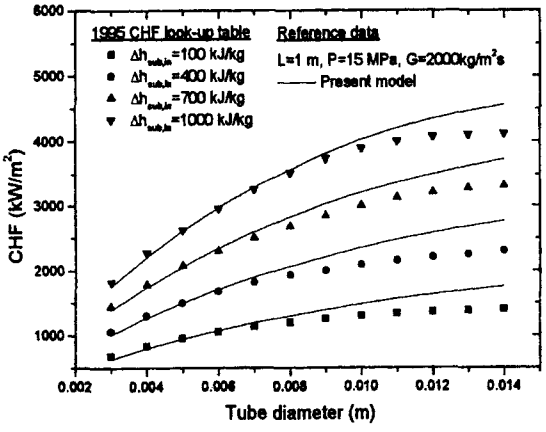

Fig. 14. Prediction of Tube Diameter Effect on CHF Compared with the 1995 CHF Look-up Table

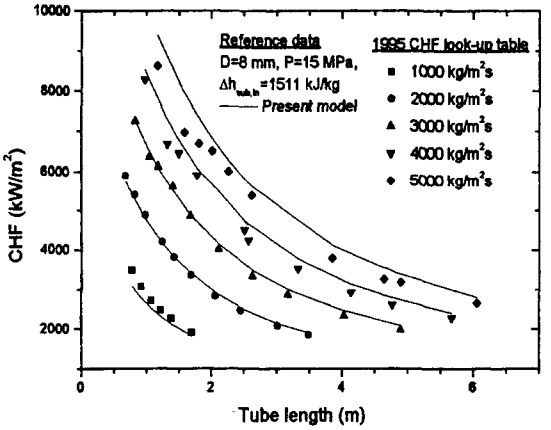

Fig. 15. Prediction of Heated Length Effect on CHF Compared with the 1995 CHF Look-up Table

tubes, a diameter correction factor for CHF is used to extend the applications to other values of tube diameter. Groeneveld et al. provided the following relationship between the CHF and the tube diameter based on fixed local conditions:

$$\frac{CHF_D}{CHF_{D=8mm}} = \left(\frac{D}{8}\right)^{-1/2} \tag{27}$$

where CHF_D is the CHF for a diameter of interest, $CHF_{D=8mm}$ is the CHF for an 8-mm tube, and D is the tube diameter in mm. However, it has been recognized that the diameter effect on CHF is very complex. For small tube diameters, the prediction by the present model agrees well with the CHF look-up table, however, the difference between two predictions increases as the tube diameter

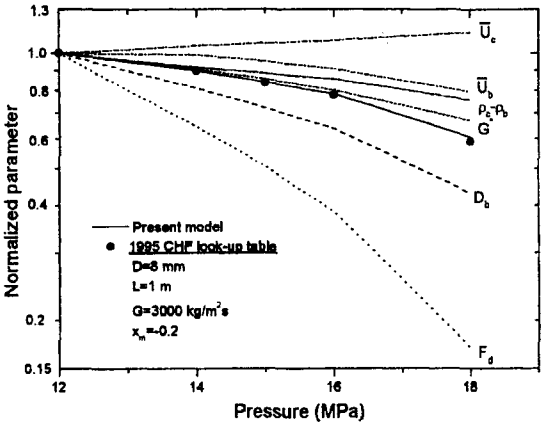

Fig. 16. Normalized Parameters as a Function of Pressure (Refernce Data : P=12 MPa, D_b=25.8μm, F_d=2.94 · 10^{-8}N, ρ_b=234kg/m^3, ρ_c=559kg/m^3, $\overline{U_b}$=2.3m/s, $\overline{U_c}$=5.42m/s, G* =14kg/m^{2}s, CHF=6.682MW/m^2)

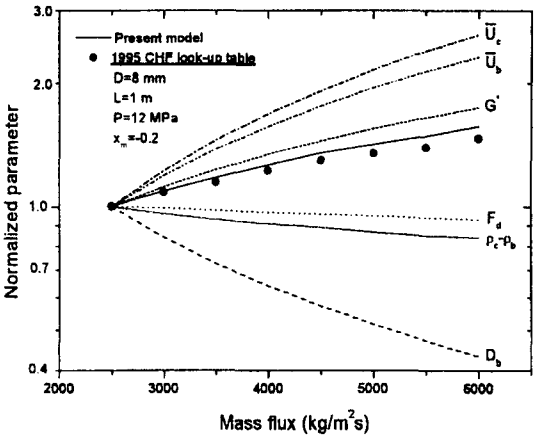

Fig. 17. Normalized Parameters as a Function of Mass Flux (Refernce Data : G=2.5Mg/m^{2}s, D_b=30.6μm, F_d=2.96 · 10^{-8}N, ρ_b=234kg/m^3, ρ_c=572kg/m^3, $\overline{U_b}$=1.93m/s, $\overline{U_c}$=4.43m/s, G* =12.5kg/m^{2}s, CHF=6.161MW/m^2)

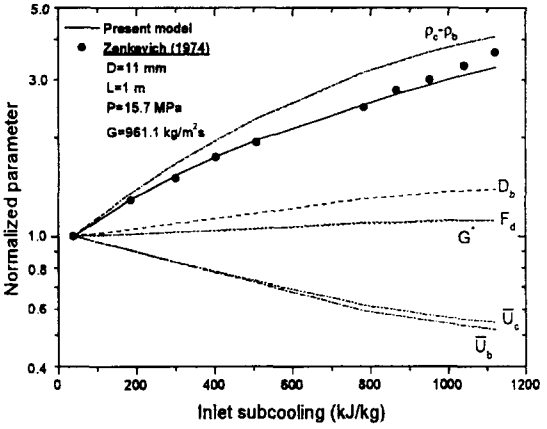

Fig. 18. Normalized Parameters as a Function of inlet Subcooling (Refernce Data: $\Delta h_{sub,in}$=40kJ/kg, D_b=38μm, F_d=1.42 · 10^{-8}N, ρ_b=191kg/m^3, ρ_c=264kg/m^3, $\overline{U_b}$=1.51m/s, $\overline{U_c}$=3.68m/s, G* =4.5kg/m^{2}s, CHF=0.766MW/m^2)

increases.

It is a general understanding that CHF is a decreasing function of tube length for fixed inlet conditions. The present model follows well the general trends of experimental data as shown in Fig. 15. It is noted that data points shown in the figure are only for the cases where the 1995 CHF look-up table data are available with a heat balance equation. The CHF decreases more rapidly for short tubs and the length effect seem to disappear for longer tubes.

The parametric trends shown in Figs. 12-15 demonstrate that the present model provides a reliable accuracy in predicting independent CHF variations with respect to mass flux, pressure, inlet subcooling, tube diameter, and tube length.

Finally, Figs. 16-18 present the normalized parameters involved in the present CHF calculation, which shows the dependence of important physical parameters as a function of (a) pressure, (b) mass flux, and (c) inlet subcooling. The normalized parameters are: the wall bubbly layer thickness or equivalent bubble diameter D_b, the frictional drag exerted on a single wall-attached bubble F_d, the limiting transverse mass flux at the outer edge of the wall bubbly layer G*, the density difference ρ_c-ρ_b, and the average velocities of the

wall bubbly layer ($\overline{U_b}$) and core ($\overline{U_c}$). The reference values of parameters for each case are included in the caption of figure. The bubble diameter decreases as pressure and mass flux increase, while it increases as inlet subcooling increases, which is determined by Eq. (19). The dominating influence of F_d results in a decrease of CHF with increasing pressure in Fig. 16. While the dominant parameter resulting in an increase of CHF with increasing mass flux is G^* in Fig. 17. The trends of other parameters are consistent with the general understanding.

4. Discussion

It is suggested here that the lateral coalescence of bubbles on the heated wall can take place if the void fraction in the wall bubbly layer reaches a certain critical value as heat flux approaches CHF. The effect of coalescence will eventually result in formation of large vapor clots followed by drastic increase of the dry spot area on the heated wall. The CHF formula of Eq.(11) allows the prediction of the CHF as functions of fluid transport properties and geometry parameters. It should be noted that the present model is valid only when the average bulk void fraction at the location of CHF occurrence is not greater than 0.8, because the flow structure assumed in this model can not be maintained for a high quality flow region.

The present model takes into account the convective shear effect due to the drag force on the wall-attached bubbles, which represents the characteristic parameter for the turbulent interchange between the wall bubbly layer and core. Even though the constitutive relations employed in the model are based on the simplifying assumptions, it is interesting to see that the CHF model agrees well in comparison with the experimental data. The result comes from the fact that the main contribution to subcooled and low quality flow boiling CHF normally caused by the limiting transverse mass interchange at the outer edge of the wall bubbly layer, which is well described by the local momentum balance equation in the present model.

The basic problem inherent in the bubble crowding model, including the present model, is that there are insufficient data to accurately specify the α_b. We have phenomenologically described the CHF mechanism in the subcooled and low quality flow boiling, however, basic mechanisms forming the constitutive models adopted here are so complicated that many uncertainties and inaccuracies might be included in the CHF model. Some of these constitutive models could be incorrect, which would naturally bias the choice of the arbitrary α_b . Considering the current state-of-the-art in the models of subcooled flow boiling followed by the CHF and the relevant experimental database, it is not possible to synthesize a mechanistic model with complete generality in the present time. However, assuming the validity of the functional forms of the constitutive relations employed in the present model, we may optimize the choice of the α_b in collaboration with available experimental CHF data. We have ignored the microscopic phenomena such as bubble dynamics on the heated wall, and statistical variations in bubble size and population density. The basis of the α_b may be derived from the theoretical investigation with aid of the experimental observation in the future.

Future work must examine the applicability of the present model to other fluids and to wider ranges of the experimental data, especially at low pressure range. Future work will also include applications to non-uniformly heated channels. Since Eq. (11) is composed of local variables, the case of a non-uniformly heated tube can be dealt with in a straightforward manner based on

the local condition hypothesis of CHF. If the total heat flux which can be fed to the tube, before the CHF location, with non-uniform heating is the same as for a uniformly heated tube of the same bore and heated length, then the predicted values of CHF will be the same. For both cases, same thermo-physical parameters will be calculated because of the same average bulk void fractions.

5. Conclusions

As a conclusion, a two-phase model has been developed to predict the CHF during the subcooled and low quality flow boiling in a uniformly heated vertical tube. Employing a simple empirical correlation of the critical wall-void fraction, the present model predicts the experimental CHF data with a good accuracy over a wide range of LWR operating conditions. The dominant mechanism controlling the CHF in the subcooled and low quality flow boiling might be properly represented in the present model. It is suggested that refinement of this model should be continued in the future to improve the critical wall void fraction. Furthermore, improvement in the current model can readily be made if better constitutive laws are used for the complex boiling phenomena.

Acknowledgements

The authors wish to express their gratitude to Dr. K. W. Lee (Korea Power Engineering Company) and Dr. W. P. Baek (Korea Advanced Institute of Science and Technology) for their precious help in preparation of this work. This work was performed under the Long-term Nuclear R&D Program sponsored by the Ministry of Science and Technology.

Nomenclature

A cross-section area (m^2)
b density ratio defined by Dix
C_{pf} specific heat (J/kgK)
C_o distribution parameter
D tube diameter (m)
D_b detached bubble diameter (m)
F skin friction factor
F_d drag force on a single bubble (N)
F_q fraction of heat flux producing vapor
G axial mass flux (kg/m^2s), $G_b=\rho_b U_b$, $G_c=\rho_c U_c$
G^* limited transverse mixing mass flux (kg/m^2s)
g acceleration due to gravity (m/s^2)
h enthalpy (kJ/kg)
h_s single phase heat transfer coefficient (W/m^2K)
h_{fg} latent enthalpy of vaporization (kJ/kg)
k thermal conductivity (W/mK)
N_{bub} number of bubble
P pressure (MPa)
Pr Prandtl number
q'' heat flux (kW/m^2)
Re Reynolds number
U local velocity (m/s)
U^+ dimensionless velocity
$\overline{U}$ mean velocity (m/s)
V_{gj} drift velocity (m/s)
x flow quality
x_{em} thermal equilibrium quality at tube exit
y distance in radial direction (m)
Y^+ dimensionless distance
Y_B^+ dimensionless distance to tip of vapor bubble
z axial location (m)

Greek letters

α void fraction,
β blockage factor
ϵ roughness size (m)
γ volume quality defined in Dix model

η_c fraction of cross-section occupied by core
λ skin friction coefficient
μ viscosity (Ns/m^2) or average mean value
ρ density (kg/m^3)
σ surface tension (N/m) or sample standard deviation
τ shear stress (N/m^2)
τ_w apparent wall shear stress (N/m^2)
$\tau_{w,v}$ viscous shear stress on wall (N/m^2)
ξ perimeter (m)
Φ_{acc} acceleration term

Subscripts

avg average
b bubbly layer
bc from bubbly layer to core
c core
cb from core to bubbly layer
CHF CHF location
d bubble detachment position
f saturated liquid
g saturated vapor
i interface of wall bubbly layer and core
in inlet
l liquid phase
sub subcooled
w heated wall
2ϕ two-phase mixture flow

References

1. J. Weisman, "The Current Status of Theoretically Based Approaches to the Prediction of the Critical Heat Flux in Flow Boiling," *Nucl. Tech.*, **99**, 1 (1992).
2. Y. Katto, "Critical Heat Flux," *Int. J. Multiphase Flow*, **20**, Suppl., 53 (1994).
3. G. P. Celata, "Modeling of Critical Heat Flux in Subcooled Flow Boiling," Convective Flow and Pool Boiling Conference, Kloster Irsee, Germany, May 18-23 (1997).
4. H. S. Kwon, T. H. Chun, S. D. Hong, D. H. Hwang, and C. Park, "Assessment of Performances and Research Status of Theoretical CHF Models in Forced Convection Boiling," *Journal of the Korean Nuclear Society*, **27**, 918 (1995).
5. J. Weisman and B. S. Pei, "Prediction of Critical Heat Flux in Flow Boiling at Low Qualities," *Int. J. Heat Mass Transfer*, **26**, 1463 (1983).
6. S. H. Ying and J. Weisman, "Prediction of the Critical Heat Flux in Flow Boiling at Intermediate Qualities," *Int. J. Heat Mass Transfer*, **29**, 1639 (1986).
7. J. Weisman and S. Ileslamlou, "A Phenomenological Model for Prediction of Critical Heat Flux under Highly Subcooled Conditions," *Fusion Tech.*, **13**, 654 (1988).
8. C. H. Lee and I. Mudawar, "A Mechanistic Critical Heat Flux Model for Subcooled Flow Boiling Based on Local Bulk Flow Conditions," *Int. J. Multiphase Flow*, **14**, 714 (1988).
9. Y. Katto, "A Prediction Model of Subcooled Water Flow Boiling CHF for Pressure in the Range 0.1-20 MPa," *Int. J. Heat Mass Transfer*, **35**, 1115 (1992).
10. G. P. Celata, M. Cumo, A. Mariani, M. Simoncini, and G. Zummo, "Rationalization of Existing Mechanistic Models for the Prediction of Water Subcooled Flow Boiling Critical Heat Flux," *Int. J. Heat Mass Transfer*, **37**, suppl.1, 347 (1994).
11. T. Iwamura et al., "Evaluation of Mechanistic DNB Models Using HCLWR CHF Data," JAERI-M 92-033, JAERI (1992).
12. G. P. Celata, M. Cumo, and A. Mariani, "Assessment of Correlations and Models for the Prediction of CHF in Water Subcooled Flow Boiling," *Int. J. Heat Mass Transfer*, **37**, 237 (1994).
13. P. Bricard and A. Souyri, "Understanding and

Modeling DNB in Forced Convective Boiling : A Critical Review," Two-phase Flow Modeling and Experimentation, Edizioni ETS, pp.843-851 (1995).

14. S. H. Chang and K. W. Lee, "A Critical Heat Flux Model Based on Mass, Energy, and Momentum Balance for Upflow Boiling at Low Qualities," *Nucl. Eng. Des.*, **113**, 35 (1989).
15. K. W. Lee et al., "An Improved and Simplified DNB Model Based on Mass, Energy, and Momentum Balance Equations, " 5th Int. Topical Metg. on Nucl. Thermal Hydraulics, Operation, and Safety, Beijing, China (1997).
16. D. C. Groeneveld, L. K. H. Leung, P. L. Kirillov, et al., "The 1995 Look-up Table for Critical Heat Flux in Tubes," *Nucl. Eng. Des.*, **163**, 1 (1996).
17. F. C. Gunther, "Photographic Study of Surface-Boiling Heat Transfer to Water with Forced Convection," *TRANS. ASME* , **73**, 115 (1951).
18. G. J. Kirby, R. Stainiforth, and L. H. Kinneir, "A Visual Study of Forced Convection Boiling - 2. Flow Patterns and Burnout for a Round Test Section," AEEW-R-506, UKAEA, Winfrith (1967).
19. V. V. Yagov and V. A. Puzin, "Burnout under Conditions of Forced Flow of Subcooled Liquid," *Thermal Engineering*, **32**, 569 (1985).
20. P. Saha and N. Zuber, "Point of Net Vapor Generation and Vapor Void Fraction in Subcooled Boiling," Proc. 5th Int. Heat Transfer Conf., Tokyo, Japan, Vol. IV, pp. 175-179 (1974).
21. D. R. H. Beattie, "An Evaluation of Two Bubble Detachment Models for Two-phase Flow," ANS-ASME Topical Meeting on Nuclear Reactor Thermo-hydraulics, Saratoga Springs, NY., NUREG/CP-0014, p.1343 (1980).
22. D. Jia and V. E. Schrock, "A Generalized Procedure for Predicting the Pressure Drop in a Subcooled Boiling Channel," 4th Miami Int. Sym. on Multi-phase Transport and Particular Phenomenon (1986).
23. S. Lu and D. Jia, "A New Method for Predicting the Pressure Drop in a Subcooled Boiling Channel," Experimental Heat Transfer, Fluid Mechanics, and Thermodynamics, edited by R. X. Shah, R. N. Ganic, and K. T. Yang, Elsevier Science Publishing Co., Inc., (1988).
24. C. K Chen, "Characteristics of Turbulent Flow Resistance in Pipes Roughened with Hemispheres," Ph.D thesis, Washington State University (1971).
25. R. P. Taylor and B. K. Hodge, "Validated Heat-Transfer and Pressure-Drop Prediction Methods Based on the Discrete Element Method: Phase I, Three-Dimensional Roughness," ANL/ESD/TM-31, Argonne National Laboratory (1992).
26. F. W. Staub, "The Void Fraction in Subcooled Boiling; Prediction of the Initial Point of Net Vapor Generation," *J. Heat Transfer*, **90**, 151 (1968).
27. D. R. Beattie and P. B. Whalley, "A Simple Two Phase Frictional Pressure Drop Calculation Method," Int. *J. Multiphase Flow*, **8**, 83 (1982).
28. S. Levy, "Forced Convection Subcooled Boiling - Prediction of Vapor Volumetric Fraction," Int. *J. Heat Mass Transfer*, **10**, 951 (1967).
29. S. C. Lee, H. Dorra and S. G. Bankoff, "A Critical Review of Predictive Models for the Onset of Significant Void in Forced-Convection Subcooled Boiling," HTD-Vol.217, Fundamentals of Subcooled Flow Boiling, ASME, pp. 33-39 (1992).

30. R. M. Nedderman and C. J. Shearer, "Correlation for the Friction Factor and Velocity Profile in the Transition Region for Flow in Sand-Roughened Pipes," *Chem. Eng. Sci.*, **19**, 423 (1964).
31. G. C. Park, "The Prediction of Void Fraction in the Subcooled Boiling Region," *Journal. of the Korean Nuclear Society*, **16**, 195 (1984).
32. R. T. Lahey, Jr. and F. J. Moody, The Thermal-Hydraulics of a Boiling Water Nuclear Reactor, American Nuclear Society, second ed., La Grange Park, Illinois (1993).
33. G. E. Dix, "Vapor Void Fractions for Forced Convection with Subcooled Boiling at Low Flow Rates," NEDO-10491, General Electric Company (1971).
34. N. Zuber and J. Findlay, "Average Volumetric Concentration in Two-Phase Flow System," *J. Heat Transfer*, **87**, 453 (1965).
35. S. H. Chang, W. P. Baek, and S. K. Moon et al., The KAIST CHF Data Bank (Rev.3), KAIST-NUSCOL-9601 (1996).
36. K. M. Becker, G. Strand et al., "Round Tube Burnout Data for Flow of Boiling Water at Pressure between 30 and 200 bar," Report KTH-NEL-14 (1971).
37. F. Mayinger, "Investigation into the Critical Heat Flux in Boiling Water," EUR-3347 (1967).
38. B. Thompson and R. V. Macbeth, "Boiling Water Heat Transfer in Uniformly Heated Round Tubes: A Compilation of World Data with Accurate Correlations," AEEW-R-356 (1964).
39. L. S. Tong, "DNB (Burnout) Studies on an Open Lattice Core," Westinghouse report WCAP-3736 (1964).
40. A. Zenkevich, "Analysis and Generalization of Experimental Data on Heat Transfer Crisis Associated with Forced Convection of Cooling Water in Tubes," AECL-Tr-Misc-304 (1974).
41. D. Hall and I. Mudawar, "Evaluation of Subcooled Critical Heat Flux Correlations Using the PU-BTPFL CHF Database for Vertical Upflow of Water in A Uniformly Heated Round Tube," Nucl. Tech., **117**, 234 (1997).
42. Y. M. Kwon and S. H. Chang, "A Mechanistic Critical Heat Flux Model for Subcooled Flow Boiling Using A Rough-Wall Analogy of Wall-Attached Bubbles," 2nd Int. Symp. On Two-phase Flow Modeling and Experimenta-tion, Italy, May (1999).
43. R. J. Weatherhead, Nucleate Boiling Characteristics and the Critical Heat Flux Occurrence in Sub-cooled Axial Flow Water System, ANL-6675 (1963).

Appendix I

CHF Calculation Procedure

Required input parameters : D, L, P, G, $\Delta h_{sub,in}$ (or h_{in}).

(1) Assume a value for q''.

(2) Calculation of $\Delta h_{sub,d}$, where all physical properties are calculated at saturated state at the system pressure.

$$Y_B^+ = 0.015\frac{(\sigma_f D \rho_f)^{1/2}}{\mu_f}$$

if $0 \le Y_B^+ \le 5$, $\Delta h_{sub,d} = q''\left[\frac{C_{pf}}{h_s} - \frac{\mathrm{Pr}_f Y_B^+}{G\sqrt{f/8}}\right]$

if $5 < Y_B^+ \le 30$, $\Delta h_{sub,d} = q''\left[\frac{C_{pf}}{h_s} - \frac{5}{G\sqrt{f/8}}\left[\mathrm{Pr}_f + \ln\left(1 + \frac{\mathrm{Pr}_f Y_B^+}{5} - \mathrm{Pr}_f\right)\right]\right]$

if $Y_B^+ > 30$, $\Delta h_{sub,d} = q''\left[\frac{C_{pf}}{h_s} - \frac{5}{G\sqrt{f/8}}\left[\mathrm{Pr}_f + \ln(1+5\mathrm{Pr}_f) + \frac{1}{2}\ln\left(\frac{Y_B^+}{30}\right)\right]\right]$

where

$$f = 0.0055\left[1 + \left(20000\frac{\varepsilon}{D} + \frac{10^6}{\mathrm{Re}_f}\right)^{1/3}\right] \quad \text{with } \varepsilon/D = 10^{-4}$$

$$h_s = 0.023\,\mathrm{Re}_f^{0.8}\,\mathrm{Pr}_f^{0.4}\left(k_f / D\right) \text{ with } \mathrm{Re}_f = \frac{GD}{\mu_f} \text{ and } \mathrm{Pr}_f = \frac{C_p\mu_f}{k_f}$$

(3) Calculation of x_d and z_d.

$$x_d = \frac{-\Delta h_{sub,d}}{h_{fg}},$$

$$z_d = \frac{GD\left(h_f - \Delta h_{sub,d} - h_{in}\right)}{4q''}$$

$$\text{if } \; z_d < 0 \; ; \; z_d = 0 \; \text{ and } \; x_d = \frac{-\Delta h_{sub,in}}{h_{fg}}$$

(4) Calculation of x_{avg} and α_{avg} at the tube exit

$$x_{avg} = \frac{x_{em} - x_d \exp(x_{em}/x_d - 1)}{1 - x_d \exp(x_{em}/x_d - 1)}$$

$$\text{where } \; x_{em} = \frac{h_{avg} - h_f}{h_{fg}} \; \text{ with } \; h_{avg} = h_{in} + \frac{4q''L}{GD}$$

$$h_l = \frac{h_{avg} - h_g x_{avg}}{1 - x_{avg}}$$

$$T_l = T(P, h_l), \quad \rho_l = \rho(P, h_l), \quad \sigma_l = \sigma(T_l), \quad \mu_l = \mu(\rho_l, T_l)$$

(5) Calculation of α_{avg}

$$\alpha_{avg} = \frac{x_{avg}}{\left\{C_o\left[x_{avg} + \frac{\rho_g}{\rho_l}\left(1 - x_{avg}\right)\right] + \frac{\rho_g V_{gj}}{G}\right\}}$$

where

$$C_o = \gamma\left[1 + \left(\frac{1}{\gamma} - 1\right)^b\right] \; \text{ with } \; \gamma = \frac{x_{avg}}{\left[x_{avg} + \frac{\rho_g}{\rho_l}\left(1 - x_{avg}\right)\right]} \; \text{ and } \; b = \left(\frac{\rho_g}{\rho_l}\right)^{0.1}$$

$$V_{gj} = 2.9\left[\frac{\left(\rho_l - \rho_g\right)\sigma_l g}{\rho_l^2}\right]^{1/4}$$

(6) Calculation of D_b.

$$\mu_{2\phi} = \mu_f(1 - \alpha_{avg})(1 + 2.5\alpha_{avg}) + \mu_g\alpha_{avg}$$

$$\rho_{avg} = \frac{\alpha_{avg}\rho_g}{x_{avg}}, \quad \mathrm{Re}_{2\phi} = \frac{GD}{\mu_{2\phi}}, \quad f_{2\phi} = f(\mathrm{Re}_{2\phi})$$

$$D_b = 0.015\sqrt{\frac{8\sigma_f D\rho_{avg}}{f_{2\phi}G^2}}$$

(7) Calculation of flow properties at the tube exit

$$\eta_c = \left(\frac{D - 2D_b}{D}\right)^2$$

$$\alpha_b = 0.83 - 0.29e^{-4.71x_{em}^{1.89}}, \quad \alpha_c = \frac{1}{\eta_c}\alpha_{avg} - \frac{1 - \eta_c}{\eta_c}\alpha_b$$

$$\rho_b = \rho_f(1 - \alpha_b) + \rho_g\alpha_b, \qquad \rho_c = \rho_l(1 - \alpha_c) + \rho_g\alpha_c$$

$$x_b = \frac{\alpha_b\rho_g}{\rho_b}, \qquad x_c = \frac{\alpha_c\rho_g}{\rho_c}$$

$$h_b = h_f(1 - x_b) + h_g x_b, \qquad h_c = h_l(1 - x_c) + h_g x_c$$

(8) Calculation of average velocities

$$\frac{1}{\sqrt{\lambda}} = 3.48 - 4\log\left(\frac{2D_b}{D} + \frac{9.35}{\mathrm{Re}_{2\phi}\sqrt{\lambda}}\right)$$

$$\tau_w = \frac{\lambda G^2}{2\rho_c\eta_c^2} \qquad Y^+ = \frac{D_b\sqrt{\tau_w\rho_c}}{\mu_{2\phi}}$$

$$\text{if } \; 0 \le Y^+ < 5, \quad \overline{U}_b = 0.5Y^+\sqrt{\frac{\tau_w}{\rho_c}}$$

$$\text{if } \; 5 \le Y^+ < 30, \quad \overline{U}_b = 0.5\left(5\ln Y^+ - 3.05\right)\sqrt{\frac{\tau_w}{\rho_c}}$$

$$\text{if } \; Y^+ \ge 30, \qquad \overline{U}_b = 0.5\left(2.5\ln Y^+ + 5.5\right)\sqrt{\frac{\tau_w}{\rho_c}}$$

$$\overline{U}_c = \frac{G - \overline{U}_b\rho_b\left(1 - \eta_c\right)}{\rho_c\,\eta_c}$$

(9) Calculation of q''_{CHF}

$$F_d = \frac{\lambda\rho_c\overline{U}_c^2}{2}\left(\frac{\pi D_b^2}{4}\right)$$

$$\xi_w = \pi D, \quad \xi_i = \pi\left(D - 2D_b\right)$$

$$G^* = \left[-\left(\rho_c - \rho_b\right)g + \frac{\pi D F_d}{D_b^2(1 - \eta_c)A}\right]\frac{A\eta_c(1 - \eta_c)}{(\overline{U}_c - \overline{U}_b)\xi_i}$$

$$q''_{CHF} = G^*(h_b - h_c)\frac{\xi_i}{\xi_w}$$

If the estimated q'' in step (1) is close enough to the calculated q''_{CHF} in step (9), q'' is the critical heat flux. Otherwise, readjust q'' and return to step (1).